Electronic Supplementary Material (ESI) for Environmental Science: Atmospheres.


# Aerosol optical properties and brown carbon in Mexico City

**Armando Retama[a,*], Mariana Ramos-Cerón[b], Olivia Rivera-Hernández[b], George Allen[c], Erik Velasco[d]**

[a] Independent Researcher, Mexico City, 11800, Mexico

[b] Secretaría del Medio Ambiente de la Ciudad de México, Mexico City, 06068, Mexico

[c] Northeast States for Coordinated Air Use Management, Boston MA 02111, USA

[d] Independent Research Scientist, 118719, Singapore

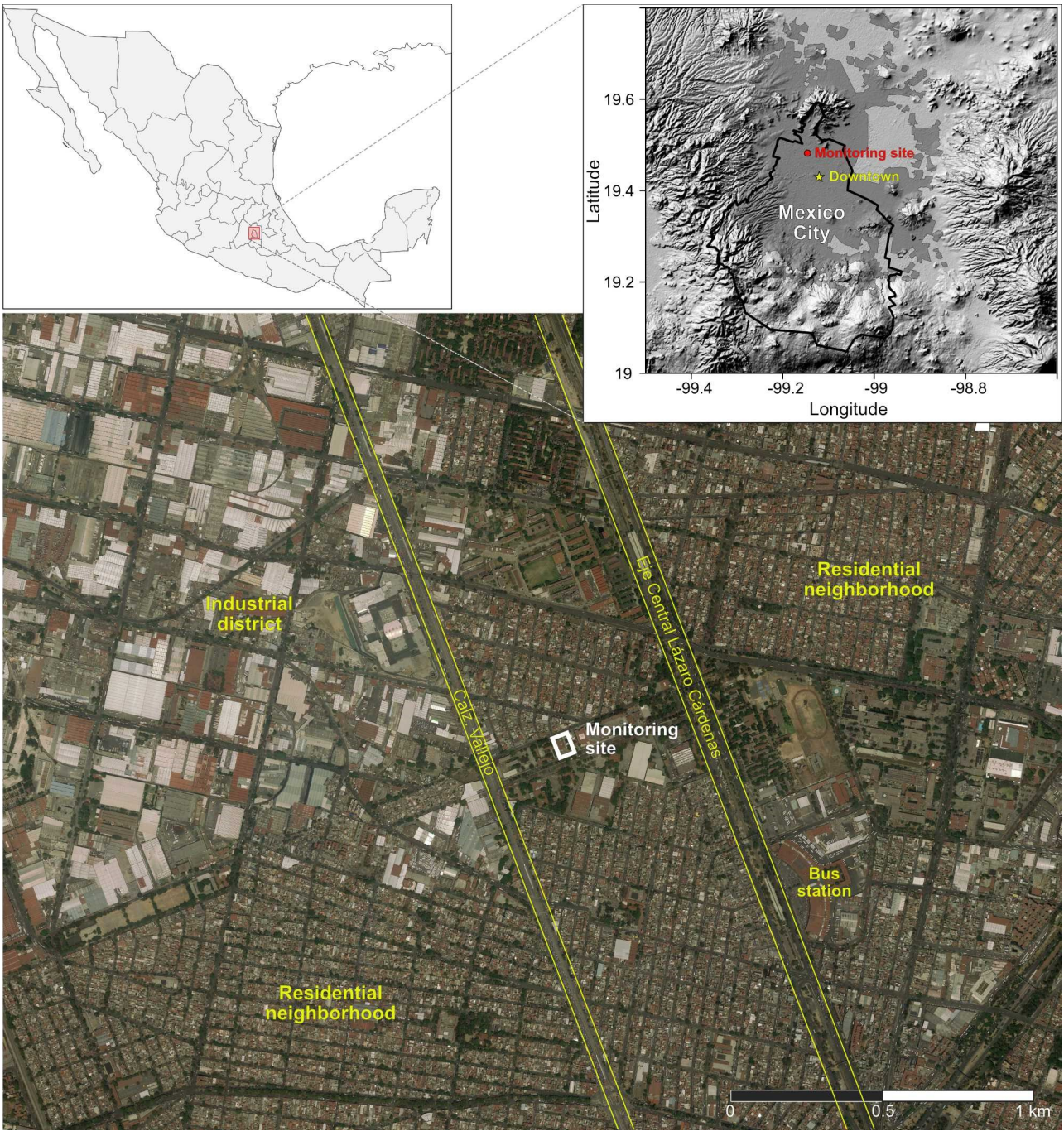


**Figure SM1.** Location of the monitoring site. The upper-left map shows the position of the Mexico City Metropolitan Area within the country. The upper-right panel shows the urban area (dark shade), political boundary of Mexico City (black contour) over the topographical relief of the basin on which the city sits, and geographical location of the Environmental Analysis Laboratory of Mexico City's Secretariat for the Environment (19º29'01.44" N, 99º08'50.21" W, 2243 m above sea level) used as monitoring site in this study; the position of the city downtown is included as reference. The main features around the monitoring site are indicated in the satellite map. Two major roads with heavy traffic located both at 500 m of the monitored site are highlighted by yellow lines.

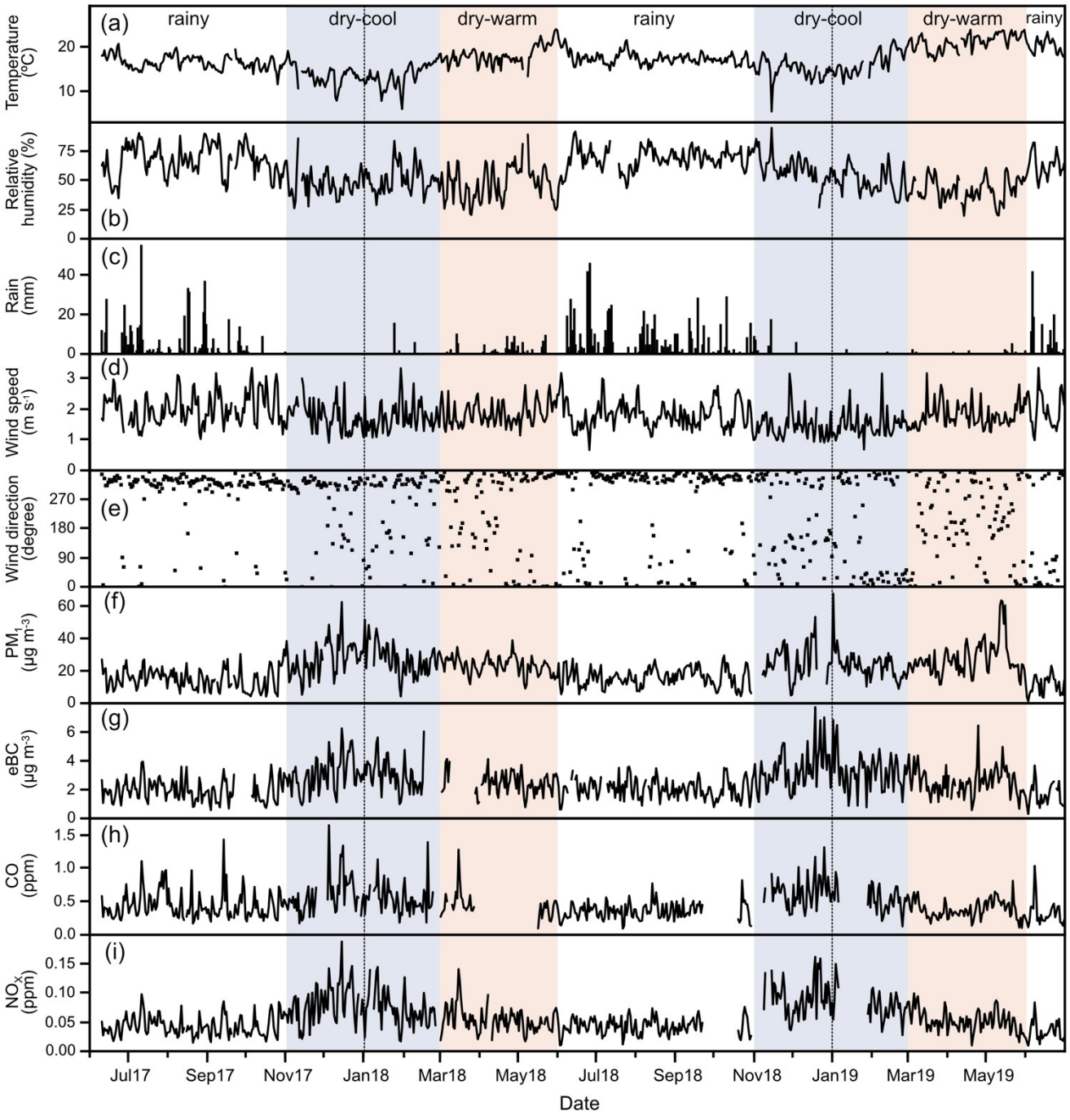


**Figure SM2.** Time series of daily arithmetic means of meteorological (a-e) and air quality (f-i) variables measured during the two-year study. Periods covering the dry-cool and dry-warm seasons are shaded in blue and pink, no shade is used for the rainy season periods.

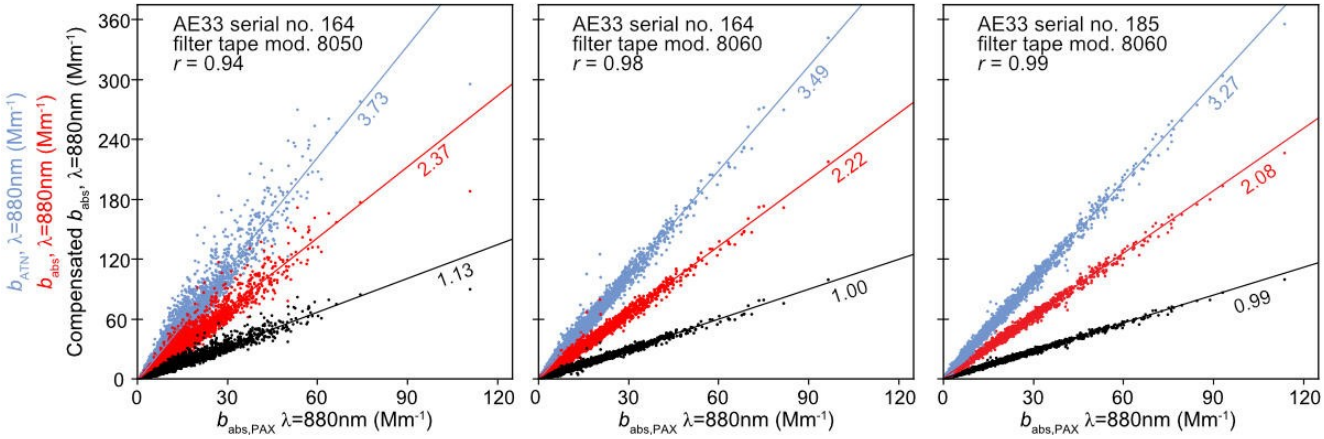


**Figure SM3**. Performance of the absorption coefficient ($b_{abs}$) at 880 nm using the correction factor, $C$, recommended by the Aethalometer's manufacturer ($b_{abs,880}$), and the individual correction factors, $C_{ref}$, obtained *in-situ* for each filter tape (compensated $b_{abs,880}$) from concurrent PAX $b_{abs}$ readings ($b_{abs\ PAX,880}$). Two similar instruments were used during the campaign, their serial number is indicated on the left upper corner. The attenuation coefficient ($b_{ATN,880}$) values yield by the Aethalometers before correction are included as reference. The slopes are included for each case per each filter tape used in this study. The three tests performed for each filter tape yielded the same Pearson's correlation coefficient (i.e., $r$ values).

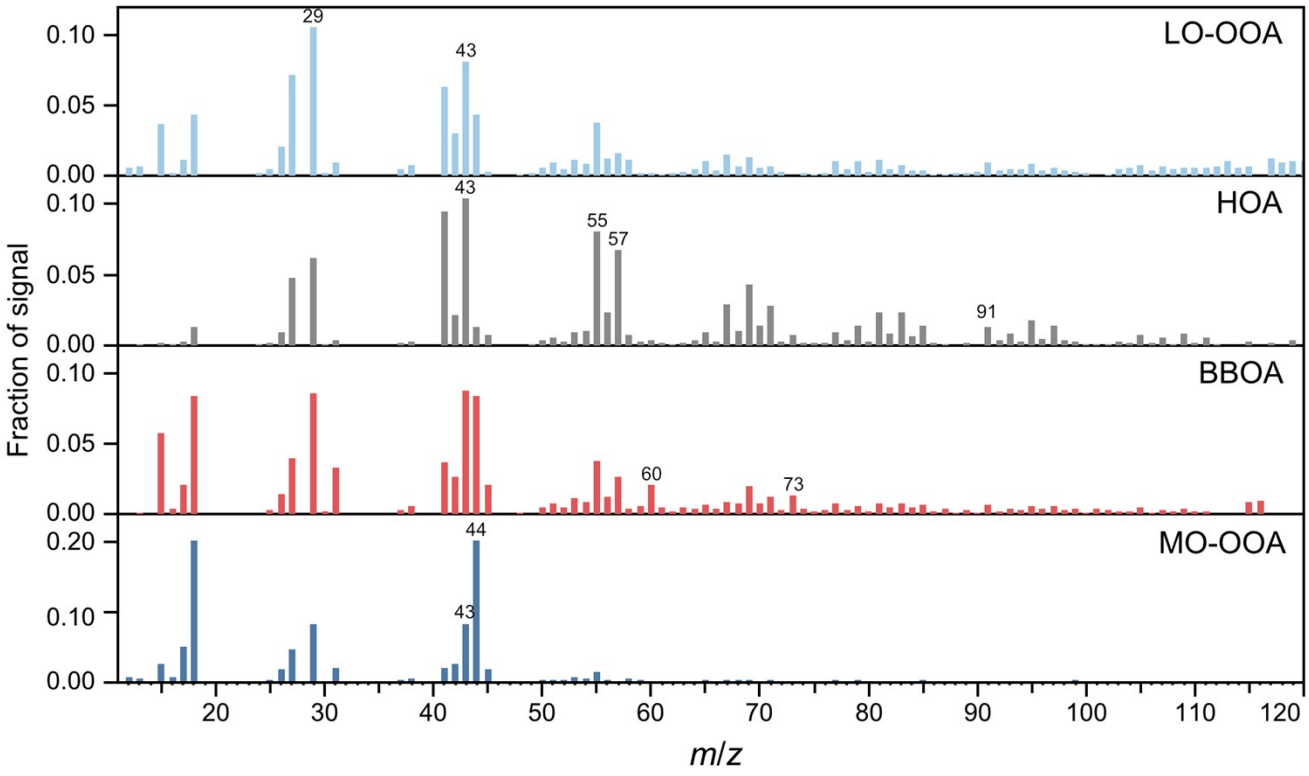


**Figure SM4.** Mass spectra profiles of the solution with four factors identified by the Positive Matrix Factorization (PMF) analysis for the organic fraction of non-refractory submicron particles measured by mass spectroscopy. Four main groups were determined: MO-OOA: more oxidized oxygenated organic aerosol; BBOA: biomass burning organic aerosol; HOA: hydrocarbon-like organic aerosol; LO-OOA: less oxidized oxygenated organic aerosol.

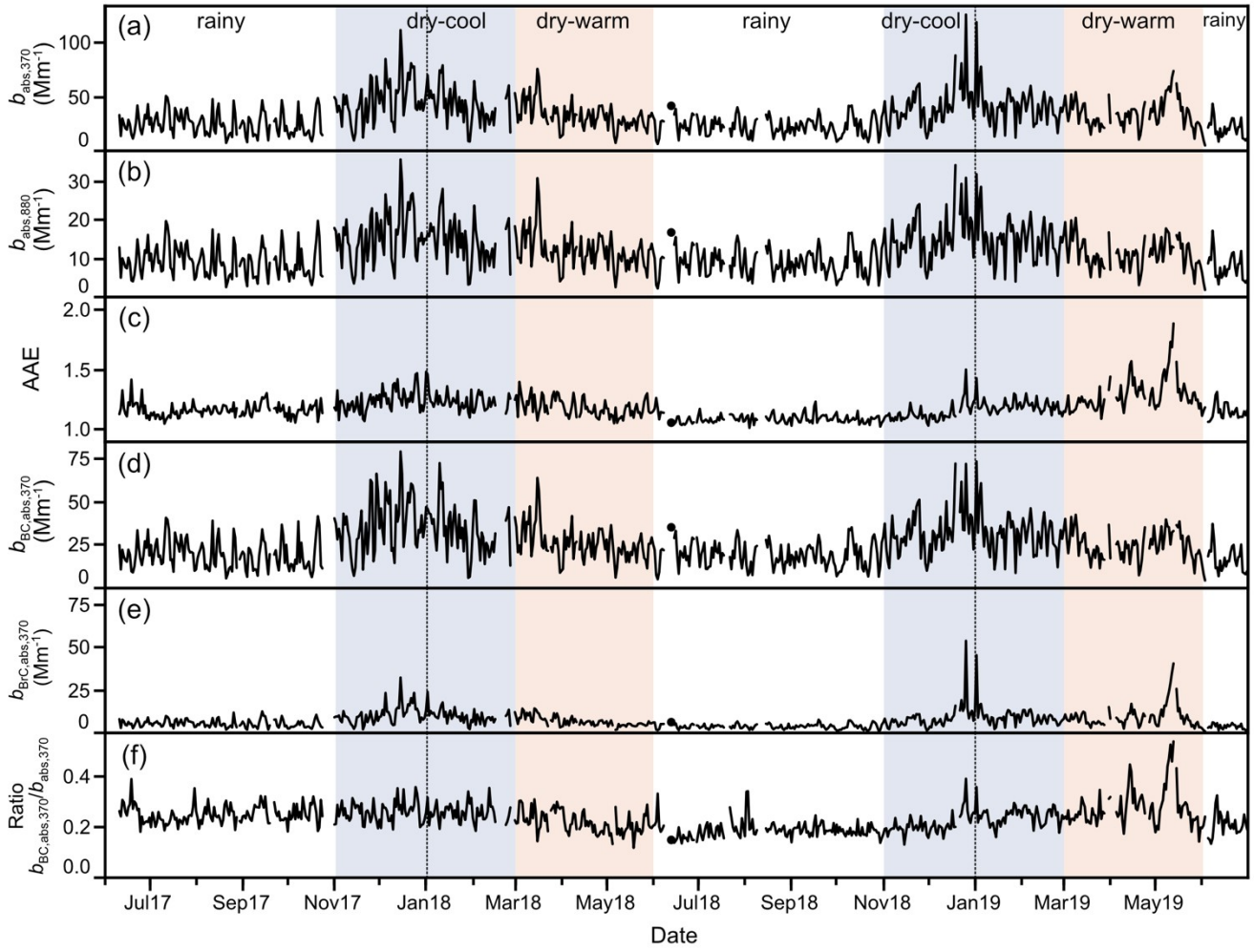


**Figure SM5**. Time series of daily arithmetic means of selected optical properties measured by the aethalometer AE33: absorption coefficient at 370 nm, $b_{abs,370}$ (a), absorption coefficient at 880 nm, $b_{abs,880}$ (b), absorption Ångström exponent, AAE (c), calculated absorption coefficient for black carbon at 370 nm, $b_{BC,abs,370}$ (d), calculated absorption coefficient for brown carbon (BrC) at 370 nm, $b_{BrC,abs,370}$ (e), and ratio between the coefficients of n BrC absorption and total absorption at 370 nm, $b_{BrC,abs,370}$ / $b_{abs,370}$ (f). Similar to previous figure, periods covering the dry-cool and dry-warm seasons are shaded in blue and pink, no shade is used for the rainy season periods.

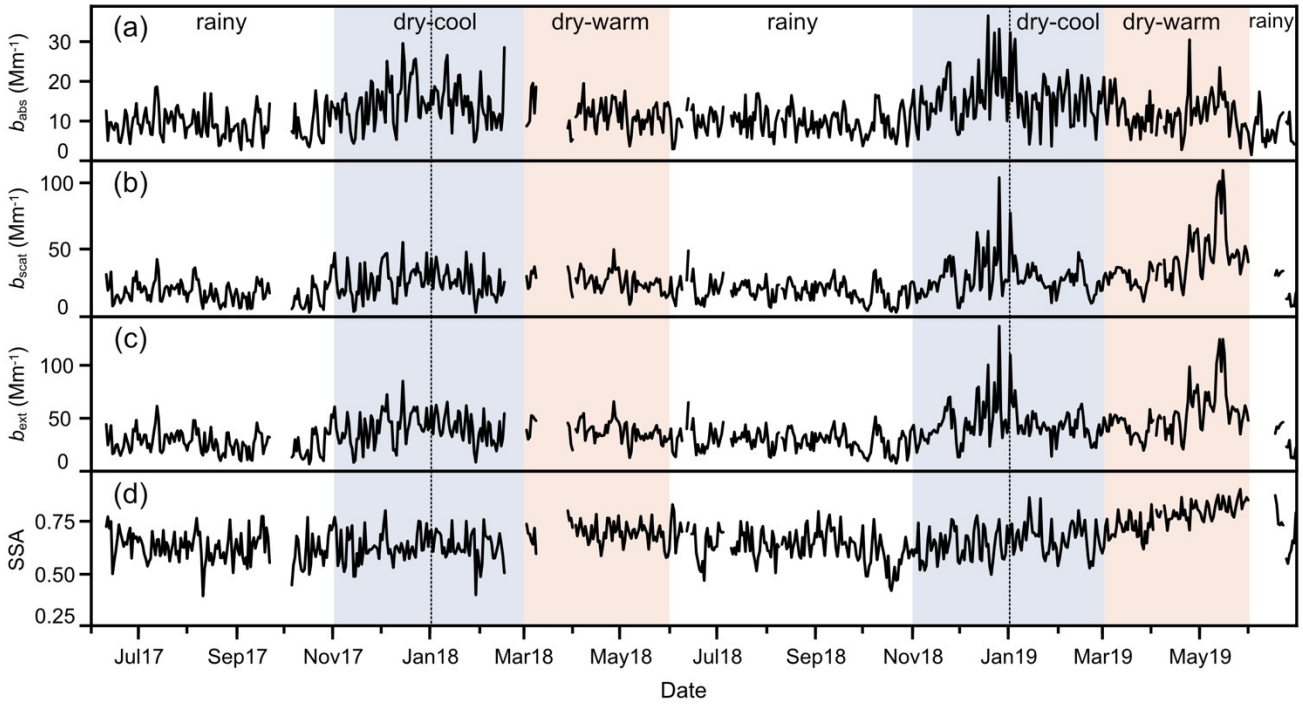


**Figure SM6.** Time series of daily arithmetic means of the optical properties measured by the PAX instrument: absorption coefficient at 870 nm, $b_{abs}$ (a), scattering coefficient at 870 nm, $b_{scat}$ (b), extinction coefficient at 870 nm, $b_{ext}$ (c) and single scattering albedo, SSA (d). Similar to previous figures, periods covering the dry-cool and dry-warm seasons are shaded in blue and pink, no shade is used for the rainy season periods.

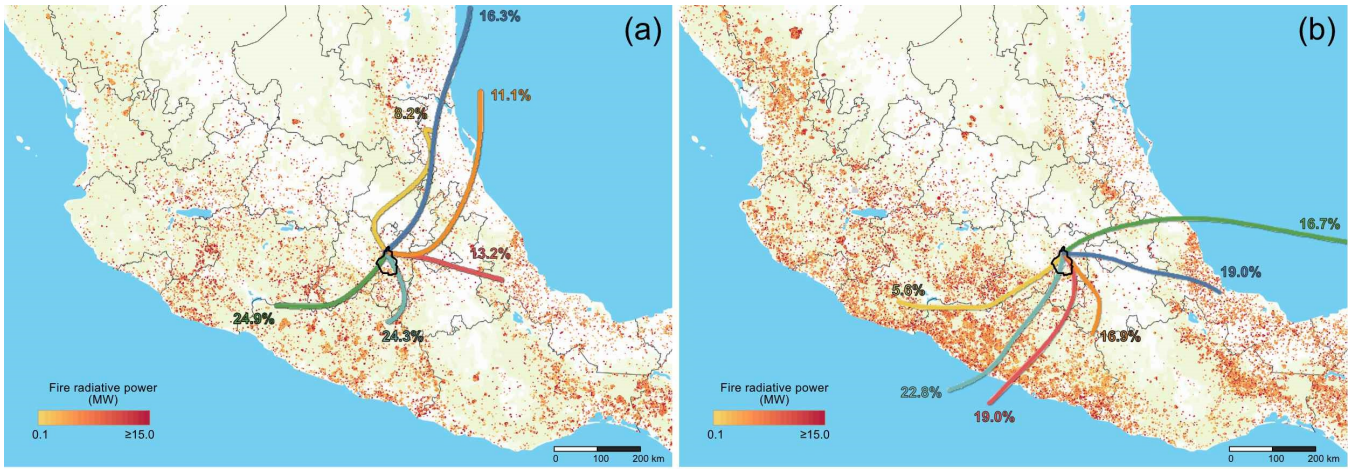


**Figure SM7.** Clusters of 36-hour backward trajectories for April 2019 (a) and May 2019 (b) when the central region of Mexico was severely affected by a massive number of wildfires. The back trajectories were obtained from the HYSPLIT application using reanalysis data, trajectories were evaluated at 100 m above ground level. Colored dots indicate the thermal anomalies (i.e., hotspots) reported by the Visible Infrared Imaging Radiometer Suite (VIIRS) and indicate potential fires, the fire radiative power is indicated by the orange to red colored scale. Six dominant clusters of trajectories were determined for each month. The percentages indicate their frequency.

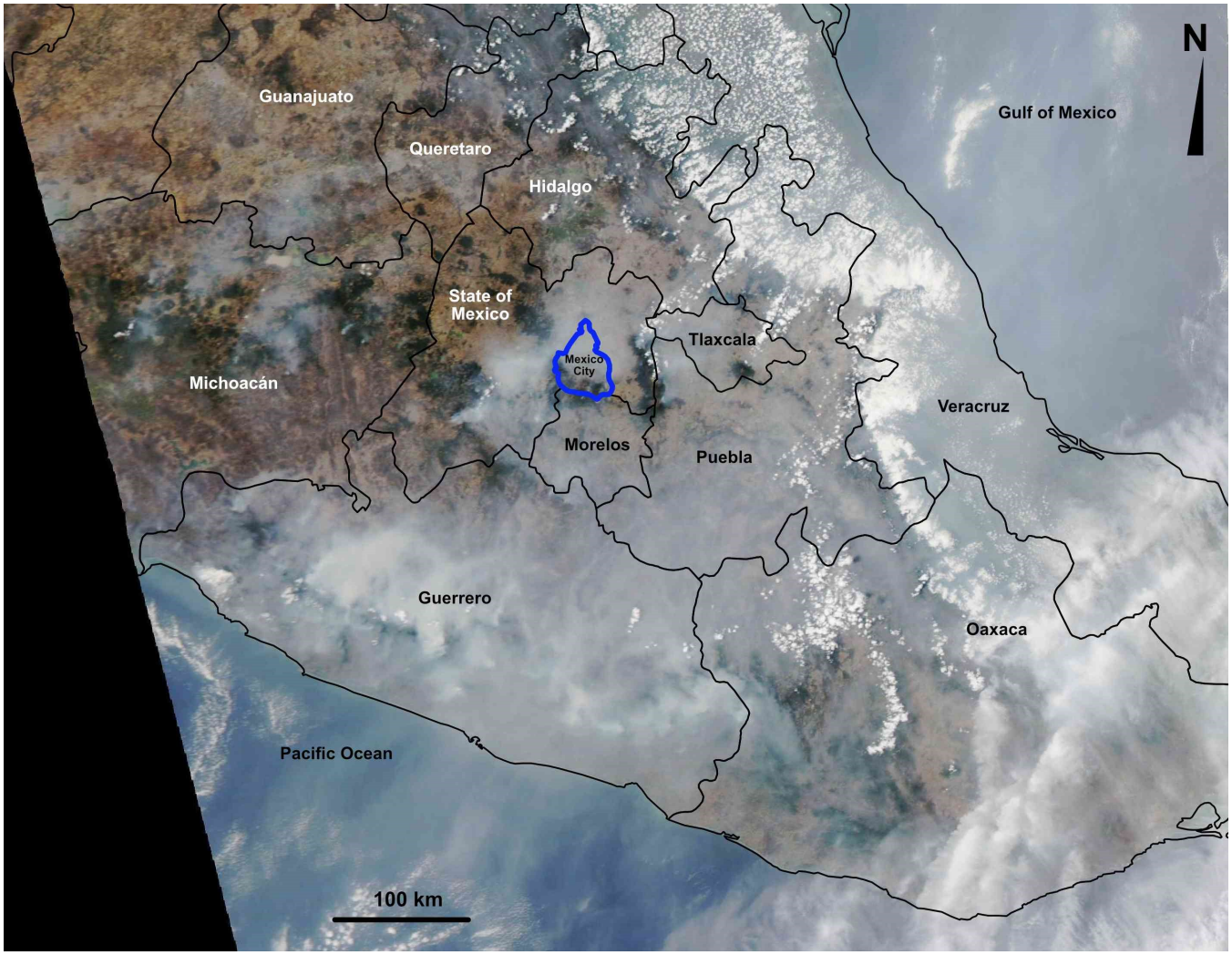


**Figure SM8.** Satellite image showing the smoke plumes produced by massive wildfires across the central region of Mexico on May 14, 2019. The blue line indicates the political boundary of Mexico City (Image: NASA / Aqua-MODIS).

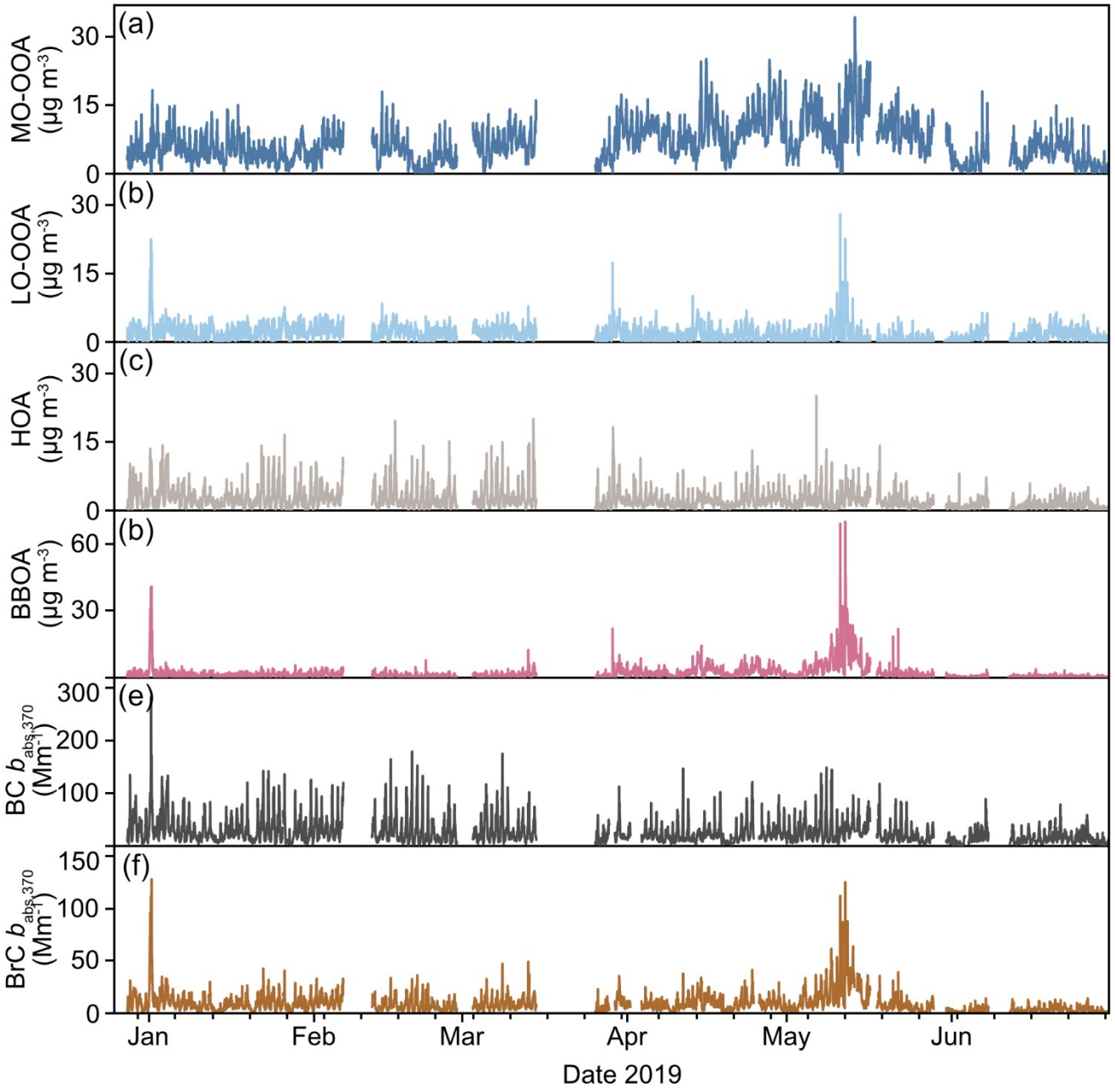


**Figure SM9.** Time series of the mass loadings obtained by the PMF analysis from the non-refractory organic aerosols measured by the Aerosol Chemical Speciation Monitor (ACSM) (a-d), and the light absorption coefficients for BC (e) and BrC (f) calculated at 370 nm. The light absorption coefficients were averaged for the same time interval used for the organic aerosol measurements. Absorption coefficients were averaged to match ACSM measurements.

**Table SM1.** Locally derived multiple-scattering correction factors ($C_{ref}$) obtained for each filter tape used by the aethalometer AE33 during the study.

| Instrument | Tape model | Period | $C_{ref}$ |
|---|---|---|---|
| AE33 164 | 8050* | 9 Jun 17 – 30 Oct 17 | 3.54 |
| AE33 164 | 8050 | 30 Oct 17 – 14 Mar 18 | 3.28 |
| AE33 164 | 8060‡ | 14 Mar 18 – 24 Sep 18 | 3.43 |
| AE33 164 | 8060 | 24 Sep 18 – 20 Dec 19 | 3.55 |
| AE33 185 | 8060 | 20 Dec 18 – 28 Jan 19 | 3.56 |
| AE33 185 | 8060 | 28 Jan 19 – 11 Jun 19 | 3.50 |
| AE33 185 | 8060 | 11 Jun 19 – 30 Jun 19 | 3.53 |

* Filter media: Pall TX40-Emfab, borosilicate glass microfibers reinforced with woven glass cloth and bonded with polytetrafluoroethylene (PTFE).
‡ Filter media: spunbonded nonwoven fabric consisting of glass fibers and polyethylene terephthalate (PET) polymerized polyester fibers.

**Table SM2.** Statistical metrics of the aerosol optical properties measured by the aethalometer AE33 and PAX instrument, and air quality and meteorological variables measured during the entire study (June 2017 – June 2019). The number of valid data ($n$) along with the geometric and arithmetic means and standard deviations ($\mu_G$ $[\sigma_G]^{\pm}$ and $\mu \pm \sigma$, respectively), median, 25th-75th percentiles, and maximum values are presented for each parameter

| Parameter | $n$ | $\mu_G$ $[\sigma_G]$ | $\mu \pm \sigma$ | Median | 25th-75th percentiles | Max |
|---|---|---|---|---|---|---|
| **Dry-warm season** (February -May) | | | | | | |
| **Aethalometer** | | | | | | |
| $b_{abs,370}$ ($Mm^{-1}$) | 4207 | 27.5 [2.0] | 34.5 ± 25.7 | 26.5 | 17.5 - 43.4 | 232.0 |
| $b_{abs,470}$ ($Mm^{-1}$) | 4207 | 20.1[2.0] | 25.5 ± 19.7 | 19.3 | 12.7 – 32.0 | 192.5 |
| $b_{abs,520}$ ($Mm^{-1}$) | 4207 | 17.2 [2.0] | 21.9 ± 17.0 | 16.4 | 10.8 - 27.4 | 170.4 |
| $b_{abs,590}$ ($Mm^{-1}$) | 4207 | 14.9 [2.0] | 19.0 ± 15.0 | 14.1 | 9.2 - 23.9 | 152.2 |
| $b_{abs,660}$ ($Mm^{-1}$) | 4207 | 12.7 [2.0] | 16.3 ± 13.0 | 12.1 | 7.9 - 20.5 | 131.5 |
| $b_{abs,880}$ ($Mm^{-1}$) | 4207 | 9.2 [2.0] | 11.9 ± 9.7 | 8.6 | 5.6 – 15.0 | 99.8 |
| $b_{abs,950}$ ($Mm^{-1}$) | 4207 | 8.5 [2.0] | 11.1 ± 9.1 | 8.0 | 5.2 – 14.0 | 93.7 |
| AAE | 4207 | 1.23 [1.14] | 1.24 ± 0.17 | 1.22 | 1.13 - 1.32 | 2.56 |
| **Photoacoustic Extinctiometer** | | | | | | |
| eBC (μg $m^{-3}$) | 3508 | 2.0 [2.0] | 2.5 ± 2.0 | 1.9 | 1.2 - 3.2 | 18.0 |
| $b_{abs,870}$ ($Mm^{-1}$) | 3508 | 9.5 [2.0] | 12.0 ± 9.3 | 8.8 | 5.9 - 14.9 | 85.3 |
| $b_{scat,870}$ ($Mm^{-1}$) | 3508 | 29.5 [1.8] | 34.9 ± 21.4 | 30.3 | 20.7 - 43.3 | 242.5 |
| $b_{ext,870}$ ($Mm^{-1}$) | 3508 | 9.5 [2.0] | 46.9 ± 26.5 | 41.8 | 5.9 - 14.9 | 256.7 |
| SSA | 3508 | 0.73 [1.18] | 0.74 ± 0.11 | 0.76 | 0.67 - 0.83 | 0.94 |
| **Air quality and meteorology** | | | | | | |
| $PM_1$ (μg $m^{-3}$) | 4120 | 22.8 [1.7] | 25.9 ± 12.7 | 24.2 | 17.3 - 32.3 | 134.8 |
| CO (ppb) | 2992 | 285.3 [2.4] | 412.4 ± 394.5 | 260.0 | 150.0 - 5300 | 3110.0 |
| $NO_X$ (ppb) | 4122 | 37.6 [2.3] | 54.1 ± 52.2 | 33.8 | 19.3 - 69.9 | 433.7 |
| Temperature (ºC) | 4207 | 19.1 [1.3] | 19.7 ± 5.0 | 19.5 | 15.7 - 23.6 | 32.6 |
| Relative humidity (%) | 4182 | 40 [2] | 45 ± 22 | 41 | 27 - 60 | 100 |
| Wind speed (m $s^{-1}$) | 4338 | 1.6 [1.8] | 1.8 ± 1.0 | 1.7 | 1.1 - 2.5 | 6.0 |
| **Rainy season** (June – October) | | | | | | |
| **Aethalometer** | | | | | | |
| $b_{abs,370}$ ($Mm^{-1}$) | 7258 | 19.8 [1.9] | 24.3 ± 16.6 | 20.0 | 12.5 - 31.2 | 140.2 |
| $b_{abs,470}$ ($Mm^{-1}$) | 7258 | 15 [1.9] | 18.5 ± 12.9 | 14.9 | 9.4 - 23.9 | 109.2 |
| $b_{abs,520}$ ($Mm^{-1}$) | 7258 | 13 [1.9] | 16.2 ± 11.3 | 13.0 | 8.1 - 20.9 | 95.3 |
| $b_{abs,590}$ ($Mm^{-1}$) | 7258 | 11.4 [2.0] | 14.2 ± 10.1 | 11.4 | 7.1 - 18.4 | 84.3 |
| $b_{abs,660}$ ($Mm^{-1}$) | 7258 | 9.8 [2.0] | 12.2 ± 8.7 | 9.8 | 6.1 - 15.8 | 71.7 |
| $b_{abs,880}$ ($Mm^{-1}$) | 7258 | 7.3 [2.0] | 9.1 ± 6.5 | 7.3 | 4.5 - 11.8 | 53.8 |
| $b_{abs,950}$ ($Mm^{-1}$) | 7258 | 6.8 [2.0] | 8.5 ± 6.1 | 6.8 | 4.2 - 11.1 | 50.3 |
| AAE | 7258 | 1.13 [1.09] | 1.13 ± 0.10 | 1.12 | 1.07 - 1.18 | 1.80 |
| **Photoacoustic Extinctiometer** | | | | | | |
| eBC (μg $m^{-3}$) | 6494 | 1.7 [1.9] | 2.0 ± 1.3 | 1.7 | 1.1 - 2.6 | 11.2 |
| $b_{abs,870}$ ($Mm^{-1}$) | 6494 | 8 [1.9] | 9.6 ± 6.3 | 7.9 | 5.2 - 12.2 | 52.9 |
| $b_{scat,870}$ ($Mm^{-1}$) | 6494 | 15.8 [2.0] | 20.0 ± 14.2 | 16.0 | 9.8 - 26.3 | 106.8 |
| $b_{ext,870}$ ($Mm^{-1}$) | 6494 | 24.9 [1.8] | 29.7 ± 17.7 | 25.1 | 16.4 - 39.1 | 131.5 |
| SSA | 6494 | 0.63 [1.25] | 0.65 ± 0.14 | 0.64 | 0.54 - 0.76 | 0.98 |
| **Air quality and meteorology** | | | | | | |
| $PM_1$ (μg $m^{-3}$) | 7490 | 12.4[2.1] | 15.6 ±10.0 | 13.3 | 8.2 - 20.7 | 95.6 |
| CO (ppb) | 6734 | 309.4[2.1] | 404.5 ± 309.0 | 310 | 190 - 540 | 3220 |

| | | | | | | |
|---|---|---|---|---|---|---|
| $NO_X$ (ppb) | 6749 | 33.5 [2.0] | 42.9 ± 32.3 | 33.4 | 19.8 - 56 | 320 |
| Temperature (ºC) | 7734 | 16.9 [1.2] | 17.3 ± 3.7 | 16.4 | 14.5 - 19.8 | 30.3 |
| Relative humidity (%) | 7544 | 64 [1] | 68 ± 21 | 71 | 53 - 84 | 100 |
| Wind speed (m $s^{-1}$) | 7654 | 1.7 [1.7] | 1.9 ± 0.9 | 1.9 | 1.3 - 2.5 | 7.0 |
| **Dry-cool season** (November – January) | | | | | | |
| **Aethalometer** | | | | | | |
| $b_{abs,370}$ ($Mm^{-1}$) | 5491 | 33.8 [2.1] | 43.6 ± 34.1 | 33.9 | 20.5 - 56.1 | 329.3 |
| $b_{abs,470}$ ($Mm^{-1}$) | 5491 | 25.0 [2.1] | 32.5 ± 25.5 | 24.9 | 14.8 - 41.8 | 241.9 |
| $b_{abs,520}$ ($Mm^{-1}$) | 5491 | 21.5 [2.1] | 28.0 ± 22.0 | 21.5 | 12.7 - 36.4 | 202.2 |
| $b_{abs,590}$ ($Mm^{-1}$) | 5491 | 18.7 [2.1] | 24.5 ± 19.3 | 18.6 | 11 - 31.8 | 171.8 |
| $b_{abs,660}$ ($Mm^{-1}$) | 5491 | 16.0 [2.1] | 20.9 ± 16.4 | 16.0 | 9.3 - 27.3 | 145.8 |
| $b_{abs,880}$ ($Mm^{-1}$) | 5491 | 11.6 [2.1] | 15.3 ± 12.1 | 11.6 | 6.8 - 20.0 | 100.3 |
| $b_{abs,950}$ ($Mm^{-1}$) | 5491 | 10.9 [2.1] | 14.3 ± 11.3 | 10.8 | 6.3 - 18.6 | 93.2 |
| AAE | 5491 | 1.20 [1.12] | 1.21 ± 0.14 | 1.19 | 1.11 - 1.27 | 1.95 |
| **Photoacoustic Extinctiometer** | | | | | | |
| eBC (µg $m^{-3}$) | 5255 | 2.5 [2.0] | 3.2 ± 2.4 | 2.5 | 1.5 - 4.2 | 24.2 |
| $b_{abs,870}$ ($Mm^{-1}$) | 5255 | 12.0 [2.0] | 15.3 ± 11.6 | 11.7 | 7.2 - 19.8 | 114.8 |
| $b_{scat,870}$ ($Mm^{-1}$) | 5255 | 23.1 [1.9] | 28.3 ± 19.2 | 24.2 | 15.3 - 35.9 | 200.5 |
| $b_{ext,870}$ ($Mm^{-1}$) | 5255 | 36.4 [1.9] | 43.5 ± 26.9 | 37.8 | 24.2 - 57.1 | 304.1 |
| SSA | 5255 | 0.63 [1.23] | 0.65 ± 0.12 | 0.65 | 0.56 - 0.74 | 0.94 |
| **Air quality and meteorology** | | | | | | |
| $PM_1$ (µg $m^{-3}$) | 5057 | 22.2 [1.9] | 26.4 ± 15.1 | 24.0 | 15.9 - 33.7 | 161.9 |
| CO (ppb) | 4250 | 425.5 [2.4] | 595.0 ± 494.1 | 430.0 | 230.0 - 830.0 | 3230 |
| $NO_X$ (ppb) | 4504 | 60.1 [2.2] | 81.1 ± 64.2 | 62.0 | 32.8 - 110.2 | 402.2 |
| Temperature (ºC) | 5530 | 13.7 [1.5] | 14.7 ± 5.1 | 14.3 | 10.9 - 18.5 | 31.0 |
| Relative humidity (%) | 5624 | 47 [2] | 52 ± 22 | 52 | 34 - 69 | 100 |
| Wind speed (m $s^{-1}$) | 5628 | 1.4 [1.9] | 1.6 ± 0.9 | 1.5 | 0.9 - 2.1 | 5.6 |

## Text SM1. Back trajectory analysis and regional fires

Mexico City it is exposed to regional emissions from forest and agriculture fires.[1] According to historical records, the entire dry season (October – June, including both dry-warm and dry-cool climatological seasons) in the central region of Mexico is exposed to wildfires, especially in croplands, since open field burning is yet a common practice to remove the stubble after harvest. Figure SM8 shows clusters of dominant back trajectories over maps including surface hotspots, which indicate potential fires, for the individual climatological seasons monitored during each year of this study. The back trajectories were obtained from the HYSPLIT application of NOOA[2] using reanalysis data, trajectories were evaluated at a height of 100 m above ground level. Cluster analysis was carried out using the openair trajCluster function for the R statistical package (https://davidcarslaw.github.io/openair/reference/trajCluster.html). The hotspots or thermal anomalies were extracted from the NASA Fire Information for Resource Management System (https://firms.modaps.eosdis.nasa.gov/download/) for the Visible Infrared Imaging Radiometer Suite (VIIRS) sensor aboard the joint NASA/NOAA Suomi-National Polar-orbiting Partnership (Suomi-NPP) satellite.[3]

As expected, each climatological season depicts distinctive back trajectories clusters, and amounts and spatial distributions of hotspots. During the dry-cool season (November to February) hotspots were present in the center of the central region of Mexico, at relatively short distances from Mexico City (< 400 km), fortunately they were not so abundant, and less than 30% of the trajectories originated in adjacent regions to the city (< 200 km), but low wind speeds and low transport heights could result in important smoke plumes. North and northeast winds were predominant during this season. These winds were linked to the movement of cold air masses originated at the north of the continent (Fig. SM10a, b).

Unsurprisingly, the number of hotspots during the rainy season (May – October) was considerably much lower. Fires were present along both coasts, but not inland. Northeast and east moisty winds arrived at Mexico City basin as shown in Fig. SM10c, d. The fires along the Gulf of Mexico coast did not represented any air quality risk to Mexico City, since the distance is quite large (> 200 km), and wind speeds were favorable for plumes dilution.

A significant increase of hotspots during the dry-warm season (February - May) is evident in the central region of Mexico (Fig. SM10 e, f), and therefore the severe impact of biomass burning plumes at regional scale. The presence of anticyclonic westerly winds brought polluted air masses mainly from the west and southwest quadrants. Worsening the situation, these plumes passed over regions closer to Mexico City (< 200 km) also highly affected by fires.

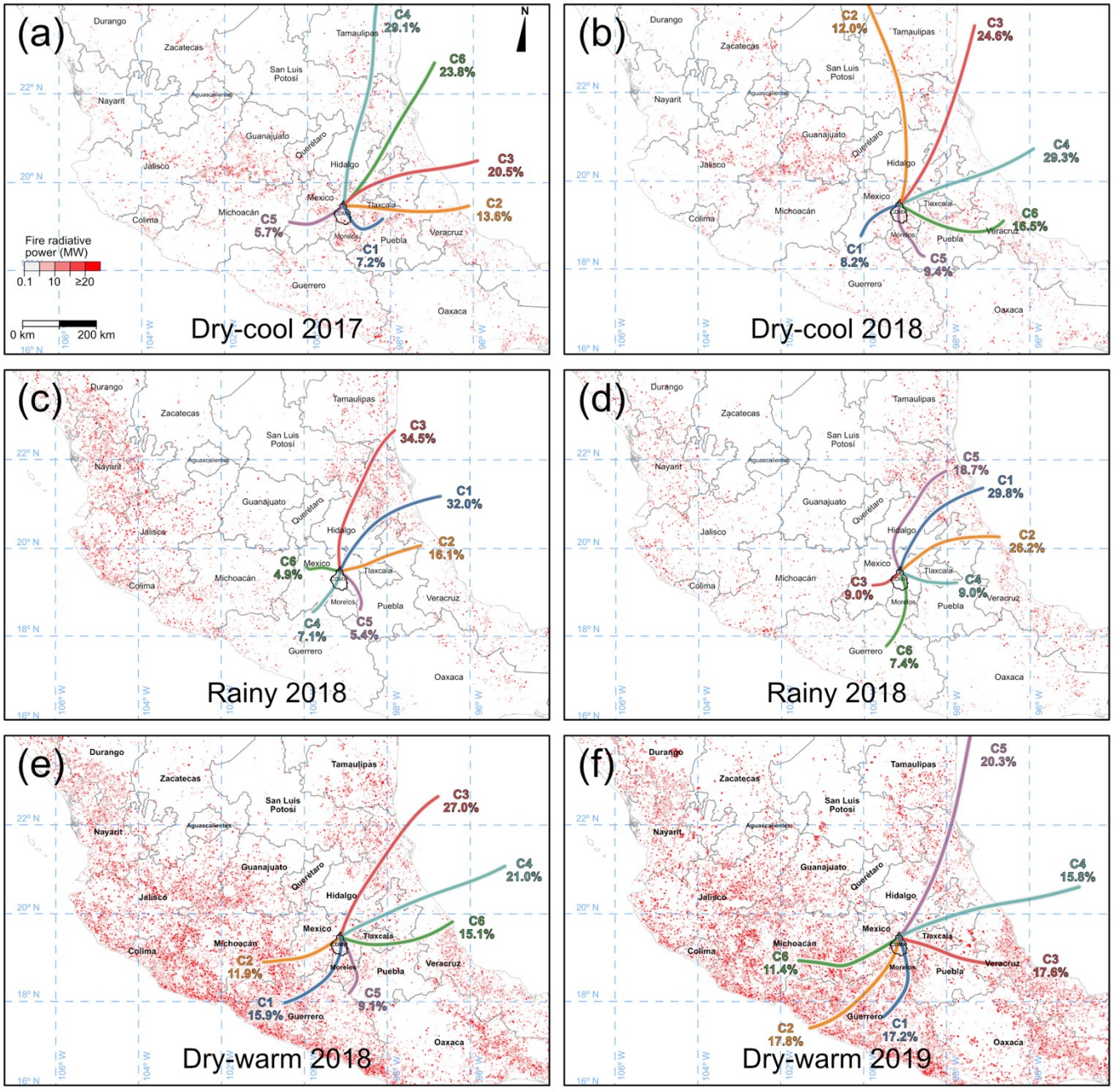


**Figure SM10.** Clusters of 36-hour backward trajectories for individual climatological season monitored during each year of this study. Red dots are thermal anomalies (i.e., hotspots) reported by the Visible Infrared Imaging Radiometer Suite (VIIRS) and indicate potential fires. Six dominant clusters of trajectories were determined for each climatological season. The percentages indicate their frequency.

## References

[1] B. Ríos, G. B. Raga. Spatio-temporal distribution of burned areas by ecoregions in Mexico and Central America, *International Journal of Remote Sensing*, 2018, 39(4), 949-970.

[2] A. F. Stein, R. R. Draxler, G. D. Rolph, B. J. B. Stunder, M. D. Cohen, F. Ngan. NOAA's HYSPLIT atmospheric transport and dispersion modeling system, *Bull. Amer. Meteor. Soc.*, 2015, 96, 2059-2077.

[3] NRT VIIRS 375 m Active Fire product VNP14IMGT. Available on-line [https://earthdata.nasa.gov/firms].